

# Landfalling Atmospheric Rivers, the Sierra Barrier Jet, and Extreme Daily Precipitation in Northern California's Upper Sacramento River Watershed

F. MARTIN RALPH

*Center for Western Weather and Water Extremes, Scripps Institution of Oceanography, University of California, San Diego, La Jolla, California*

JASON M. CORDEIRA

*Department of Atmospheric Science and Chemistry, Plymouth State University, Plymouth, New Hampshire*

PAUL J. NEIMAN

*Physical Sciences Division, NOAA/Earth System Research Laboratory, Boulder, Colorado*

MIMI HUGHES

*Physical Sciences Division, NOAA/Earth System Research Laboratory, and Cooperative Institute for Research in the Environmental Sciences, University of Colorado, Boulder, Colorado*

(Manuscript received 15 September 2015, in final form 12 April 2016)

## ABSTRACT

The upper Sacramento River watershed is vital to California's water supply and is susceptible to major floods. Orographic precipitation in this complex terrain involves both atmospheric rivers (ARs) and the Sierra barrier jet (SBJ). The south-southeasterly SBJ induces orographic precipitation along south-facing slopes in the Mt. Shasta–Trinity Alps, whereas landfalling ARs ascend up and over the statically stable SBJ and induce orographic precipitation along west-facing slopes in the northern Sierra Nevada. This paper explores the occurrence of extreme daily precipitation (EDP) in this region in association with landfalling ARs and the SBJ. The 50 wettest days (i.e., days with EDP) for water years (WYs) 2002–11 based on the average of daily precipitation from eight rain gauges known as the Northern Sierra 8-Station Index (NS8I) are compared to dates from an SSM/I satellite-based landfalling AR-detection method and dates with SBJ events identified from nearby wind profiler data. These 50 days with EDP accounted for 20% of all precipitation during the 10-WY period, or 5 days with EDP per year on average account for one-fifth of WY precipitation. In summary, 46 of 50 (92%) days with EDP are associated with landfalling ARs on either the day before or the day of precipitation, whereas 45 of 50 (90%) days with EDP are associated with SBJ conditions on the day of EDP. Forty-one of 50 (82%) days with EDP are associated with both a landfalling AR and an SBJ. The top 10 days with EDP were all associated with both a landfalling AR and an SBJ.

## 1. Introduction

The availability and management of water supply in California's north Central Valley (CV) along the upper Sacramento River is strongly influenced by variability in cool-season precipitation, snowpack, and streamflow in

the northern Sierra Nevada and Mt. Shasta–Trinity Alps regions. The California Department of Water Resources (DWR), and other water managers who seek to gauge water supply, closely monitor the precipitation in this region using daily precipitation totals averaged across eight sites known as the Northern Sierra 8-Station Index (NS8I; Fig. 1). Numerous studies suggest that a majority of cool-season precipitation in this region occurs in conjunction with winter storms and their interaction with the complex topography in association with landfalling atmospheric rivers (ARs) and terrain-locked

---

*Corresponding author address:* Jason M. Cordeira, Department of Atmospheric Science and Chemistry, Plymouth State University, 17 High St., MSC 48, Plymouth, NH 03264.  
E-mail: j\_cordeira@plymouth.edu

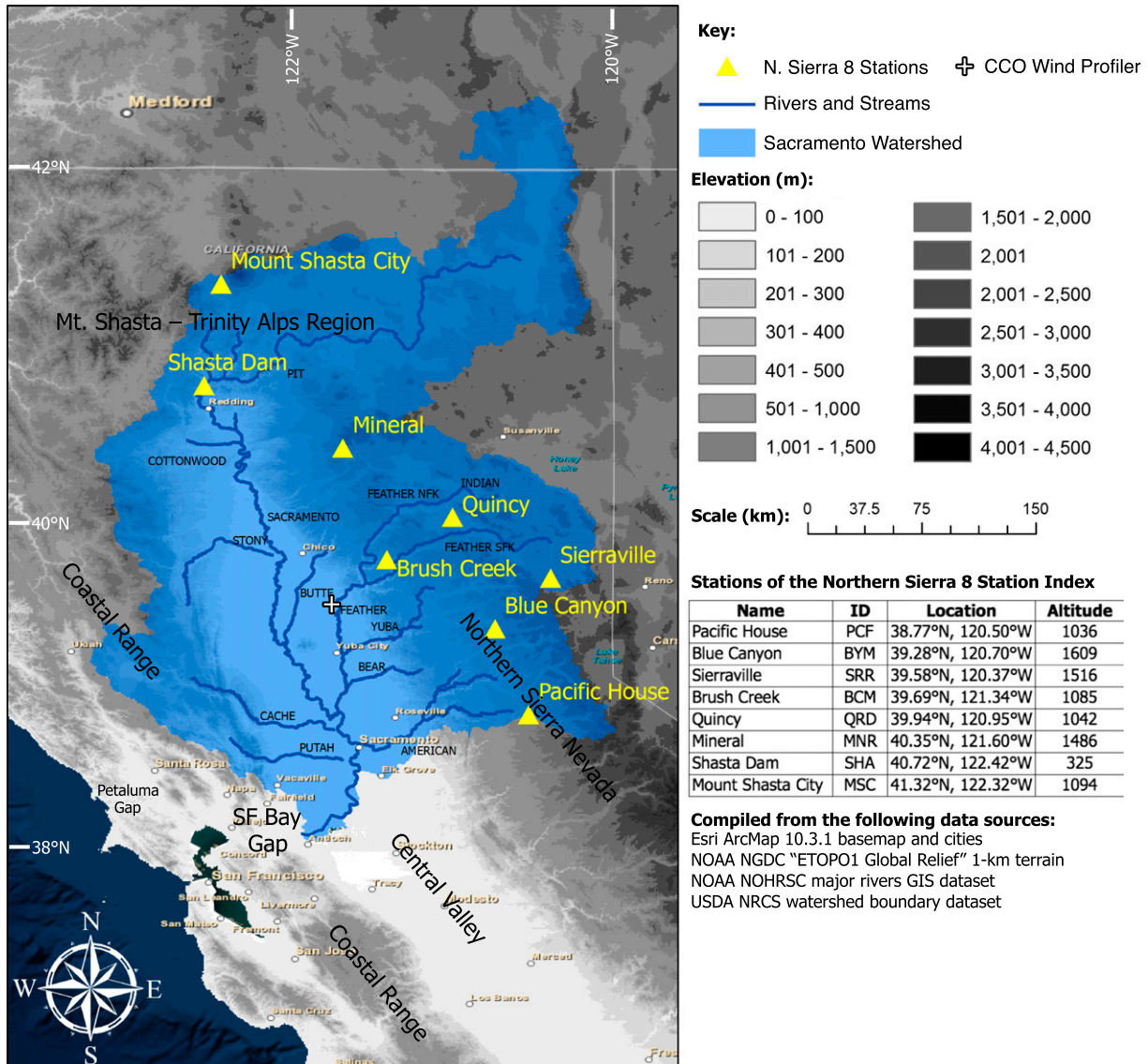


FIG. 1. The locations, IDs, and altitude (m MSL; inset table) of the eight stations that comprise the NS8I (yellow triangles) atop terrain elevation (m; shaded according to scale) and an outline of the Sacramento River watershed (blue shaded) and its tributaries (blue lines). The location of the CCO wind profiler is indicated by the white cross.

Sierra barrier jets (SBJs; e.g., [Dettinger 2004](#); [Galewsky and Sobel 2005](#); [Ralph et al. 2006, 2011, 2013a](#); [Kim and Kang 2007](#); [Reeves et al. 2008](#); [Guan et al. 2010](#); [Lundquist et al. 2010](#); [Smith et al. 2010](#); [Neiman et al. 2008b, 2010, 2013, 2014](#); [Dettinger et al. 2011](#); [Kim et al. 2012](#); [White et al. 2015](#)). The overarching objective of this study is to collectively identify what fraction of days with extreme daily precipitation (EDP) in the NS8I occurs in association with ARs and SBJs.

Atmospheric rivers are long (thousands of kilometers) and narrow (~500 km) regions of enhanced integrated water vapor (IWV) and integrated water vapor transport (IVT) located in the warm sector of transient

midlatitude cyclones (e.g., [Zhu and Newell 1998](#); [Ralph et al. 2004, 2006](#); [Neiman et al. 2008a,b](#)). ARs typically represent regions of lower-tropospheric water vapor flux along a pre-cold-frontal low-level jet (e.g., [Ralph et al. 2004](#)). SBJs are a mountain-parallel core of locally strong winds composed primarily of ageostrophic flow at ~1 km AGL ([Parish 1982](#)). The SBJ forms in response to the deceleration of stably stratified westerly flow as it approaches the west slope of the Sierra Nevada. This deceleration of westerly flow leads to a lower-tropospheric acceleration of a southerly ageostrophic wind and a core of Sierra-parallel (~160°) winds along the windward slope beneath Sierra crest level (~3 km).

Individual case studies and composite studies of EDP across Northern California have identified that both landfalling ARs and south-southeasterly SBJs are associated with heavy orographic precipitation along the west slope of the northern Sierra Nevada and south slope of the Mt. Shasta–Trinity Alps, respectively (e.g., Neiman et al. 2010, 2013, 2014; Ralph et al. 2011; Ralph and Dettinger 2012; Kingsmill et al. 2013; White et al. 2015). A majority (75%) of water vapor flux within ARs located over the eastern North Pacific occurs within the lowest 2.25 km of the troposphere (Ralph et al. 2006), whereas a prominent peak in water vapor flux along the SBJ in the northern CV occurs at  $\sim 1.5$  km (Neiman et al. 2013). In environments often characterized by moist neutral static stability, heavy orographic precipitation often results in regions where water vapor flux along ARs and SBJs intersect mountainous terrain (Neiman et al. 2008a). The so-called “upslope IWV flux” explains up to 70% of the variance in total precipitation that results from forced saturated ascent along ARs (Ralph et al. 2006) and explains  $>80\%$  of the variance in hourly precipitation rate that occurs in association with forced saturated ascent along SBJs (Neiman et al. 2013).

The studies by Neiman et al. (2013, 2014) and Kingsmill et al. (2013) identify that ARs are capable of transporting lower-tropospheric water vapor into California’s north CV through openings in terrain over northern coastal California known as the Petaluma Gap and the San Francisco Bay Gap (Fig. 1). Once in the CV, the water vapor may either ascend and promote orographic enhanced precipitation above SBJ altitudes along the west slope of the northern Sierra Nevada or be carried northward at low altitudes ( $\sim 1$ – $2$  km) along the SBJ to later ascend and promote orographic enhanced precipitation along the south slope of the Mt. Shasta–Trinity Alps [see Fig. 13 from Neiman et al. (2013)]. The stations that comprise the NS8I are therefore ideally located along the slopes of these topographic features (Fig. 1) in order to adequately investigate what fraction of days with EDP in the NS8I occurs in association with ARs and SBJs. Based on the results of Neiman et al. (2013, 2014) and Kingsmill et al. (2013), we hypothesize that a large majority of EDP in the NS8I occurs in conjunction with both landfalling ARs and the SBJ.

The proposed hypothesis is tested through investigation of the 50 largest daily precipitation totals measured by the NS8I over a 10-water-year (WY) period from WY 2002 through WY 2011 (e.g., WY 2002 is from 1 October 2001 to 30 September 2002). Section 2 describes the data and methodology, whereas section 3 presents event statistics and composite analyses. A summarizing discussion is provided in section 4.

## 2. Data and methods

The EDP across the northern Sierra Nevada and Mt. Shasta–Trinity Alps region is identified from daily precipitation totals averaged across the eight gauges that comprise the NS8I. The NS8I is available online from the DWR California Data Exchange Center (<http://cdec.water.ca.gov/cdecapp/precipapp/get8SIPrecipIndex.action>). The EDP is defined in this study as the 50 days with the largest daily precipitation totals during WYs 2002–11, representing a manageable number of days to evaluate and the wettest  $\sim 1.37\%$  of daily precipitation totals during this period.

Landfalling ARs are identified following the methodology used to create a catalog of ARs described by Neiman et al. (2008b) that uses a Special Sensor Microwave Imager (SSM/I; Hollinger et al. 1990) satellite-based IWV detection method (Wentz 1995) that was first used by Ralph et al. (2004). This methodology includes a subjective identification of ARs using objective criteria that require narrow plumes of IWV with values  $>2$  cm that are  $>2000$  km long and  $<1000$  km wide to intersect the U.S. West Coast between  $32.5^\circ$  and  $41.0^\circ$ N (Fig. 2a; see Neiman et al. 2008b). The presence of an AR meeting these criteria is noted on either the day of EDP or the day prior in order to account for the low-temporal-resolution (twice-daily composites of the polar-orbiting swaths valid for 0000–1200 UTC and 1200–2400 UTC) observations from the SSM/I instrument. The results were relatively insensitive to the choice of defining AR conditions on the day of EDP versus both the day of EDP and the day prior. The SBJs are identified from data collected from a 915-MHz radar wind profiler (Carter et al. 1995) located at Chico, California (CCO), that was deployed by the NOAA/Earth Systems Research Laboratory as part of the Hydrometeorology Testbed–West (Ralph et al. 2013b). The SBJs are identified using the Neiman et al. (2010) methodology that requires 1) a Sierra Nevada–parallel ( $160^\circ$ ) wind speed  $V_s > 12 \text{ m s}^{-1}$  below 3 km, 2) a maximum  $V_s$  located at  $\geq 200$  m AGL, and 3) a  $V_s$  that decreases by  $>2 \text{ m s}^{-1}$  between the level of maximum  $V_s$  and 3 km (Fig. 2b). Presence of an SBJ meeting these criteria is solely noted on the day of EDP.

Composite analyses are constructed from the North American Regional Reanalysis (NARR; Mesinger et al. 2006) for the 50 days with EDP in order to illustrate water vapor flux along landfalling ARs and south-southeasterly SBJs. The NARR contains data with 32-km horizontal grid spacing on 45 vertical levels that are available at 3-h intervals; however, only the 0000 UTC reanalysis periods for the day with EDP are used in this study. Although the grid spacing of the NARR is

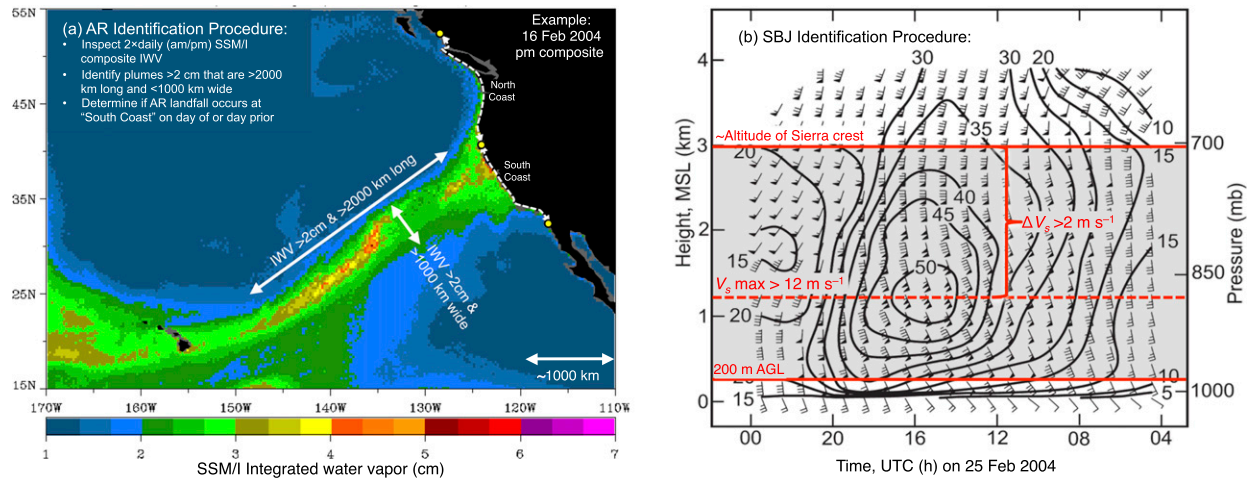


FIG. 2. (a) Annotated SSM/I satellite-based IWV (cm; shaded) on 16 Feb 2004 that illustrates the method used to detect the presence of a landfalling AR in each of the 50 days with EDP. Only ARs making landfall in California are counted [i.e., between  $32.5^{\circ}$  and  $41^{\circ}$ N as in the Neiman et al. (2008b) AR catalog]. (b) Annotated time–height section adapted from Neiman et al. (2010) of hourly averaged wind profiles (flag =  $25 \text{ m s}^{-1}$ ; barb =  $5 \text{ m s}^{-1}$ ; half barb =  $2.5 \text{ m s}^{-1}$ ) and barrier-parallel isotachs ( $\text{m s}^{-1}$ ; directed from  $160^{\circ}$ ) at CCO on 25 Feb 2004 that illustrates the method used to detect the presence of an SBJ.

sufficient for synoptic–mesoscale analysis of ARs and the SBJ (e.g., Neiman et al. 2014), it has a known positive elevation bias in the altitude of wind speed maxima along the SBJ and a negative magnitude bias in water vapor flux along the SBJ as compared to higher-resolution downscaled simulations owing to a coarse representation of terrain across Northern California (Hughes et al. 2012).

### 3. Results

#### a. Event statistics

The 50 EDP totals identified in the NS8I ranged from 43 to 103 mm, contained a mean value of 55 mm, and contributed to  $\sim 2\%$ – $7\%$  of their respective total WY precipitation (Table 1). The 50 days with EDP (1.37% of all days) accounted for 20% of all observed precipitation during the 10-WY period. In other words, 5 days with EDP per year on average account for one-fifth of WY precipitation in this region. The 50 EDP totals were part of several multiday precipitation events: 24 of 50 (45%) days with EDP occurred on consecutive days or at least twice on three consecutive days. The mean value of the highest 72-h precipitation totals that included the 24-h period with EDP from individual stations that comprise the NS8I was 210 mm; the highest 72-h precipitation total at any one station within the NS8I was 369 mm. The 72-h precipitation totals on 18 of 50 days are rainfall category 1 (R-Cat 1) precipitation events (200–300 mm), whereas 4 of 50 days are rainfall category 2 (R-Cat 2) precipitation events (300–400 mm) according to the methodology of Ralph and Dettinger (2012). Forty-eight of the 50 days

with EDP occurred during the October–March cool season, which is consistent with occurrences of heavy precipitation caused by landfalling ARs identified by Ralph and Dettinger (2012).

Forty-six of 50 (92%) days with EDP occur on the day of or the day after a landfalling AR is identified at the coast in SSM/I imagery (i.e., AR conditions exist on the day of or the day prior to EDP), whereas 43 of 50 (86%) days with EDP occur solely on the day of a landfalling AR. Forty-five of 50 (90%) days with EDP occur on days with an SBJ identified at CCO in profiler data, and 41 of 50 (82%) days with EDP occur on days with both a landfalling AR and SBJ. All 50 days with EDP occur on days with either a landfalling AR or SBJ. The 10 days with the largest EDP totals all occur on days with both a landfalling AR and SBJ. Section 3b explores the synoptic- and mesoscale processes associated with landfalling ARs and SBJs related to EDP.

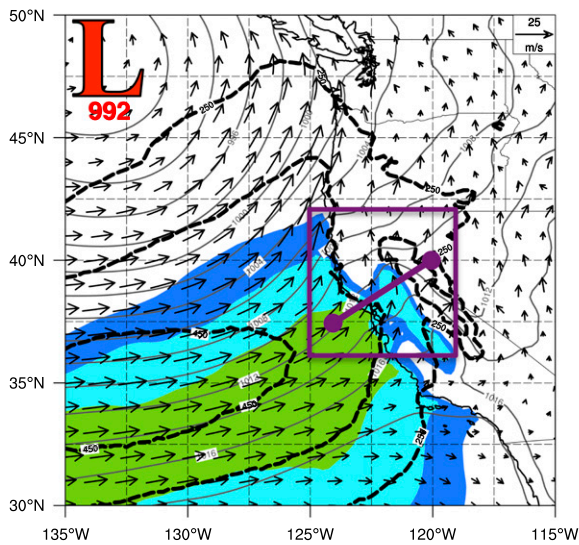
#### b. Composite analysis

Composite analysis of the IWV, IVT, sea level pressure, and 900-hPa winds (Figs. 3a,b) illustrates that the 50 days with EDP occurred in conjunction with an occluded low pressure center (992 hPa) located over the northeast Pacific near  $48^{\circ}\text{N}$ ,  $133^{\circ}\text{W}$ . The warm sector of this occluded cyclone contained broad westerly-to-southwesterly 900-hPa flow  $>10 \text{ m s}^{-1}$  in an environment with IWV values  $>2.4 \text{ cm}$  and IVT magnitudes  $>450 \text{ kg m}^{-1} \text{ s}^{-1}$  that spans from near Hawaii (not shown) to the central California coast (Fig. 3a). The composite IWV and IVT structures suggest that this feature is an AR with a length scale

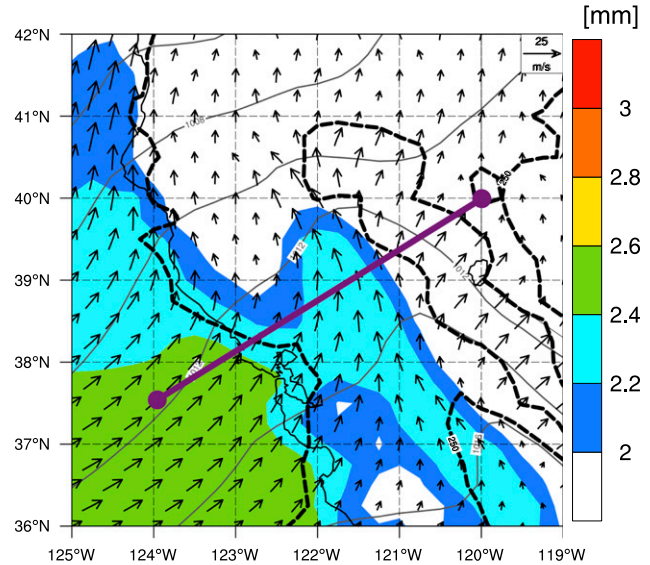
TABLE 1. Dates and characteristics of the 50 days with EDP within the NS8I. Characteristics include the 24-h precipitation, 24-h precipitation as a percentage of WY precipitation, AR landfall on the day of EDP or the day prior, SBJ on the day of EDP, the maximum 72-h precipitation at any of the eight stations, the 72-h precipitation as a percent of WY precipitation, and the R-Cat designation following the methodology of [Ralph and Dettinger \(2012\)](#). The 10 wettest days with EDP are indicated with an asterisk.

Date	NS8I 24-h precip (mm)	24-h precip (% WY)	AR? (Yes or No)	SBJ? (Yes or No)	Max 72-h station precip (mm)	R-Cat of max 72-h precip (0–4)
24 Nov 2001	46	3.8	Yes	Yes	120	0
2 Dec 2001	50	4.1	Yes	Yes	180	0
2 Jan 2002	44	3.6	Yes	Yes	105	0
8 Nov 2002*	76	5.0	Yes	Yes	180	0
13 Dec 2002	59	3.9	Yes	Yes	369	2
14 Dec 2002*	103	6.8	Yes	Yes	369	2
15 Dec 2002	55	3.6	No	Yes	369	2
16 Dec 2002*	65	4.3	Yes	Yes	349	2
27 Dec 2002	43	2.9	Yes	Yes	228	1
28 Dec 2002	54	3.6	Yes	Yes	228	1
14 Mar 2003	47	3.1	Yes	Yes	154	0
15 Mar 2003	58	3.8	Yes	Yes	154	0
6 Dec 2003	48	4.0	Yes	Yes	177	0
24 Dec 2003	50	4.2	Yes	Yes	128	0
29 Dec 2003	44	3.7	Yes	Yes	172	0
1 Jan 2004	43	3.6	Yes	Yes	122	0
16 Feb 2004	43	3.6	Yes	Yes	281	1
17 Feb 2004*	72	6.0	Yes	Yes	281	1
26 Feb 2004	53	4.4	Yes	Yes	176	0
7 Dec 2004	46	3.1	Yes	Yes	245	1
8 Dec 2004*	71	4.8	Yes	Yes	245	1
30 Dec 2004	45	3.1	No	Yes	196	0
18 May 2005	48	3.3	Yes	Yes	178	0
1 Dec 2005*	66	3.2	Yes	Yes	218	1
2 Dec 2005	43	2.1	Yes	Yes	189	0
21 Dec 2005	48	2.4	Yes	No	260	1
22 Dec 2005	57	2.8	Yes	Yes	260	1
26 Dec 2005	44	2.2	Yes	Yes	173	0
28 Dec 2005*	63	3.1	Yes	Yes	243	1
30 Dec 2005	49	2.4	Yes	Yes	299	1
31 Dec 2005*	99	4.8	Yes	Yes	299	1
27 Feb 2006*	66	3.2	Yes	Yes	184	0
28 Feb 2006	59	2.9	Yes	No	184	0
3 Apr 2006	49	2.4	Yes	Yes	162	0
10 Feb 2007	51	5.4	Yes	Yes	262	1
4 Jan 2008	50	5.4	Yes	Yes	160	0
5 Jan 2008	46	5.0	Yes	No	160	0
1 Nov 2008	50	4.1	No	Yes	157	0
23 Feb 2009	60	4.8	Yes	Yes	181	0
2 Mar 2009	59	4.8	Yes	Yes	194	0
3 Mar 2009	47	3.8	Yes	No	194	0
14 Oct 2009	55	3.9	Yes	Yes	150	0
18 Jan 2010	48	3.4	Yes	Yes	204	1
19 Jan 2010	47	3.3	Yes	Yes	204	1
24 Oct 2010*	97	5.1	Yes	Yes	269	1
18 Dec 2010	57	3.0	Yes	Yes	226	1
19 Dec 2010	44	2.3	Yes	No	226	1
16 Mar 2011	46	2.4	Yes	Yes	139	0
19 Mar 2011	50	2.6	No	Yes	141	0
20 Mar 2011	45	2.4	Yes	Yes	141	0
Top 10 counts			10/10	10/10		
Top 50 counts			46/50	45/50		

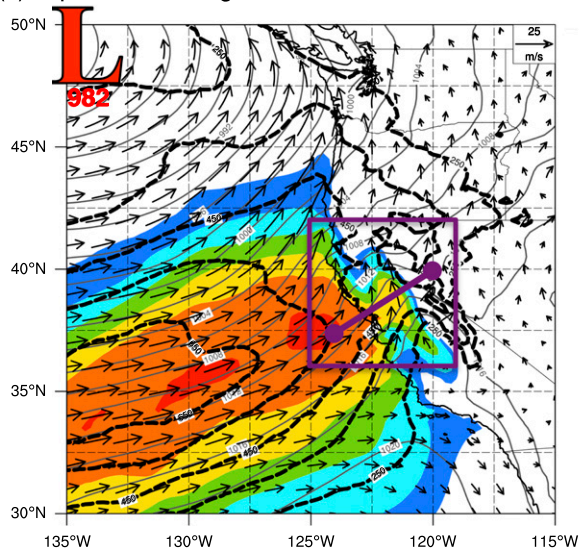
(a) Top 50 EDP: Large Domain



(b) Top 50 EDP: Zoomed Domain



(c) Top 10 EDP: Large Domain



(d) Top 10 EDP: Zoomed Domain

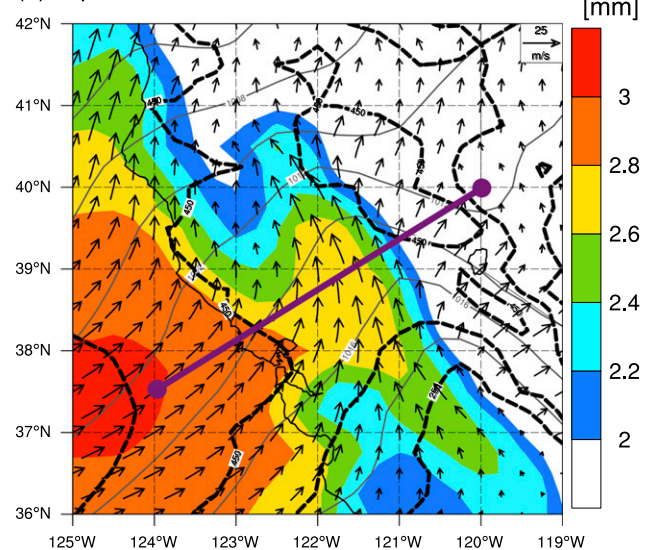


FIG. 3. NARR composite of the (a),(b) 50 days and (c),(d) top 10 days with EDP that illustrate IWV (cm; shaded according to scale), sea level pressure (gray contours every 2 hPa), IVT magnitude (dashed contours every  $100 \text{ kg m}^{-1} \text{ s}^{-1}$  beginning at  $250 \text{ kg m}^{-1} \text{ s}^{-1}$ ), and 900-hPa total wind ( $\text{m s}^{-1}$ ; reference vector in upper right of each panel). Zoomed-in areas of (a) and (c) over the northern CV are given in (b) and (d). The red “L” notes the composite location and intensity of the sea level pressure minimum. The purple cross-sectional line is for Fig. 4. The purple squares in (a) and (c) are the boundaries for (b) and (d).

of  $>2000 \text{ km}$  and a width of  $\sim 1500 \text{ km}$ . Note that inspection of the IWV and IVT structure from individual cases highlights a more characteristic width of  $<1000 \text{ km}$ ; thus, the large composite width is the effect of averaging over many events with differing spatial structures. The IWV along this composite AR is transported to the northeast along a streamline oriented  $\sim 230^\circ$  through the San Francisco Bay Gap (Fig. 1) and into the northern CV (Fig. 3b). The SBJ is observed in this

composite analysis as a backing of  $\sim 7.5 \text{ m s}^{-1}$  900-hPa winds to south-southeast ( $\sim 160^\circ$ ) over and within the northern CV. For comparison purposes, the top 10 days with EDP are associated with a stronger occluded low pressure system (982 hPa) that contains more intense AR conditions with IWV values  $>3.0 \text{ cm}$  and IVT magnitudes  $>650 \text{ kg m}^{-1} \text{ s}^{-1}$  (Fig. 3c) and more intense SBJ conditions with 900-hPa south-southeasterly winds  $>10 \text{ m s}^{-1}$  (Fig. 3d).

(a) Top 50 EDP: AR-Parallel Cross Section

(b) Top 10 EDP: AR-Parallel Cross Section

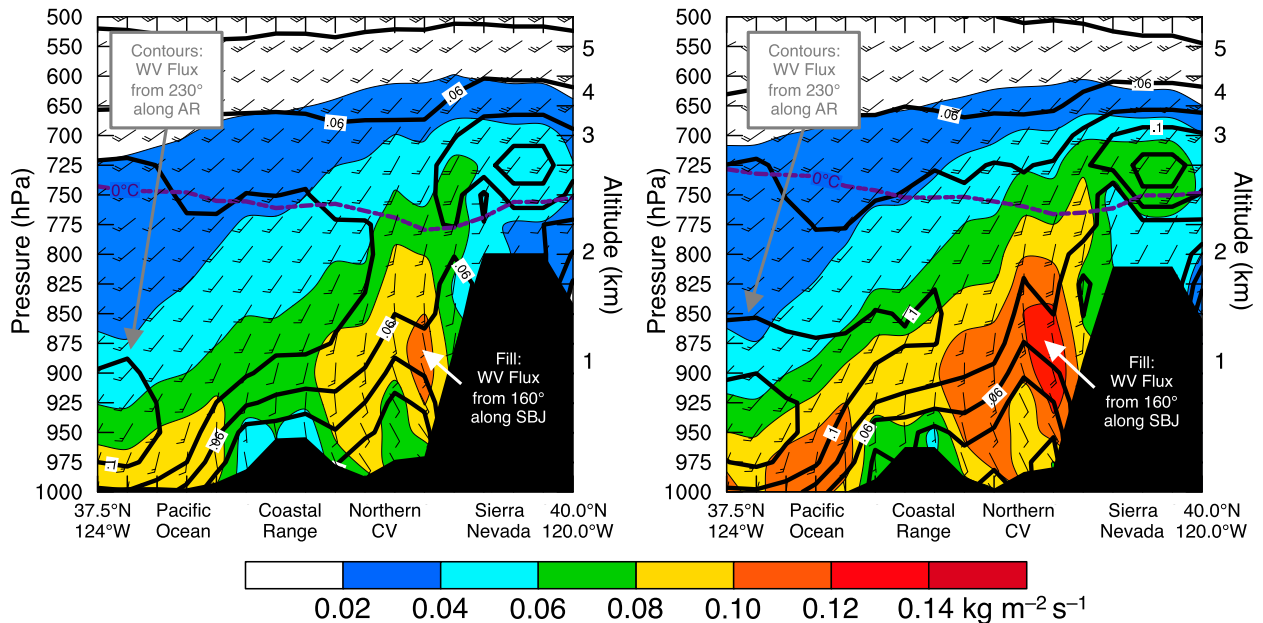


FIG. 4. Composite cross section along an AR-parallel line from 37.5°N, 124°W to 40°N, 120°W (shown in Fig. 3) of the (a) 50 days and (b) top 10 days with EDP that illustrates SBJ water vapor (WV) flux ( $\text{kg m}^{-2} \text{s}^{-1}$ ; shaded according to scale), AR WV flux (contoured every  $0.02 \text{ kg m}^{-2} \text{s}^{-1}$  beginning at  $0.02 \text{ kg m}^{-2} \text{s}^{-1}$ ), and total wind barbs (as in Fig. 2b). The SBJ WV flux is projection of total WV flux along  $160^\circ$ , whereas AR WV flux is projection of total WV flux along  $230^\circ$ .

An AR-parallel composite cross-sectional analysis that spans the northeast Pacific, Coastal Range, northern CV, and northern Sierra Nevada illustrates that the 50 days with EDP occur in association with a south-southeast total wind that is  $\sim 7.5 \text{ m s}^{-1}$  along an SBJ near 1 km over the northern CV and a west-southwest total wind that is  $\sim 7.5\text{--}10 \text{ m s}^{-1}$  farther west along the AR near 0.50 km that increases to  $>12.5 \text{ m s}^{-1}$  over the northern Sierra Nevada above 3 km (Fig. 4a). Water vapor flux along the SBJ (i.e., total water vapor flux projected onto  $160^\circ$ ) peaks near 1 km with a magnitude of  $>0.10 \text{ kg m}^{-2} \text{s}^{-1}$  along the west slope of the northern Sierra Nevada, whereas water vapor flux along the AR (i.e., total water vapor flux projected onto  $230^\circ$ ) peaks below 1 km over the northeast Pacific and again above the crest of the northern Sierra Nevada above 3 km with magnitudes  $>0.10 \text{ kg m}^{-2} \text{s}^{-1}$ .

A majority of the water vapor flux along both the AR and the SBJ occurs below the  $\sim 2.5\text{-km}$  freezing level that is located above crest level of the northern Sierra Nevada, which suggests that any precipitation in the presence of orographic ascent would fall in liquid form (Fig. 4a). The average altitude of the  $0^\circ\text{C}$  isotherm  $Z_{0^\circ\text{C}}$  over the northern CV at the grid point nearest the average location of the NS8I stations ( $39.96^\circ\text{N}$ ,  $121.28^\circ\text{W}$ ) is 2.22 km MSL, with 42 of 50 (84%) days characterized

by  $Z_{0^\circ\text{C}} > 1.61 \text{ km MSL}$  (the highest station altitude in the NS8I). The minimum  $Z_{0^\circ\text{C}}$  was 1.21 km MSL, which is higher than five of the eight stations in the NS8I (Fig. 1). These data suggest that precipitation from a few events may be associated with frozen precipitation, which could minimally contaminate the results. The  $Z_{0^\circ\text{C}}$  decreases from southwest to northeast along the cross section, which is likely associated with a combination of latent cooling via melting precipitation, adiabatic cooling via ascent, and sensible cooling via hydrometeor conduction (e.g., Minder et al. 2011).

The decrease in water vapor flux along the AR from the northeast Pacific into the northern CV occurs in conjunction with an inland decrease in wind speeds below 1 km, which is consistent with the observed southwest-to-northeast decrease in IVT along the AR in Fig. 3a. Alternatively, the maximum in water vapor flux along the AR above the crest of the Northern Sierra occurs in conjunction with the increase in wind speed. The increase in altitude of the water vapor flux maximum along the AR from below 1 km over the northeast Pacific to above 3 km over the northern Sierra Nevada is consistent with detailed experimental observations of water vapor flux rising over the SBJ (Kingsmill et al. 2013; Neiman et al. 2014).

For comparison purposes, the top 10 days with EDP are associated with a similar horizontal and vertical structure of water vapor flux along the AR and SBJ with magnitudes that are  $>0.12 \text{ kg m}^{-2} \text{ s}^{-1}$  (Fig. 4b). The average  $Z_{0^\circ\text{C}}$  during the top 10 days with EDP is 2.66 km MSL, with all 10 days characterized by  $Z_{0^\circ\text{C}} > 1.61$  km MSL. Note that a prominent maximum in water vapor flux from  $160^\circ$  also occurs along a lower-tropospheric coastal barrier jet that could influence orographic precipitation gradients along the Coastal Range (e.g., Lundquist et al. 2010); this topic is beyond the scope of the current investigation.

#### 4. Discussion and summary

This study investigated the 50 wettest days across the upper Sacramento River watershed and their association with landfalling ARs and SBJs during WYs 2002–11. The 50 wettest days, referred to as days with EDP, are derived from the NS8I that is used by DWR and other water managers to gauge water supply in the upper Sacramento River watershed region. A large majority of the 50 days with EDP occurred on the day of or the day after a landfalling AR (92%), on the day of an SBJ (90%), or both (82%). All 50 days with EDP occurred on days with either an AR or SBJ, and the top 10 days with EDP all occurred on days with both a landfalling AR and an SBJ.

Composite analysis of the 50 days with EDP illustrates that extreme precipitation across the northern Sierra Nevada and Mt. Shasta–Trinity Alps region is largely influenced by a west-southwesterly water vapor flux along a landfalling AR that increases in altitude from below 1 km over the northeast Pacific to  $\sim 3$  km over the northern Sierra Nevada and is locally influenced by a low-altitude south-southeasterly water vapor flux along an SBJ at  $\sim 1$  km. The horizontal and vertical structure of water vapor fluxes along landfalling ARs and SBJs on days with EDP in the NS8I complement the results from case studies and similar investigations that describe the relationships among landfalling ARs, SBJs, and precipitation distributions over the northern Sierra Nevada and Mt. Shasta–Trinity Alps regions by Kingsmill et al. (2013) and Neiman et al. (2010, 2013, 2014). The stronger values of water vapor fluxes along landfalling ARs and SBJs on the top 10 days with EDP also complement results from Ralph et al. (2006) and Neiman et al. (2010, 2013) that indicate stronger values of water vapor flux along landfalling ARs and SBJs produce more intense precipitation and higher precipitation totals.

The results presented in section 3 indicate that landfalling ARs and SBJs are important synoptic- and mesoscale processes, respectively, responsible for producing

EDP in the NS8I; however, these results do not indicate which process is necessarily more important. For example, the data in Table 1 can be used to identify that the NS8I on days with EDP is not noticeably higher or lower on days with ARs ( $N = 46$ ; 56 mm) versus days without ARs ( $N = 4$ ; 52 mm), nor is it noticeably higher or lower on days with SBJs ( $N = 45$ ; 56 mm) versus days without SBJs ( $N = 5$ ; 49 mm) or on days with both an AR and SBJ ( $N = 41$ ; 57 mm) versus days without both ( $N = 9$ ; 49 mm). Further bifurcation of the eight stations into two groups that represent the two stations along the south-facing slopes of the Mt. Shasta–Trinity Alps region and the six remaining stations along the west-facing slopes of the northern Sierra Nevada similarly did not produce noticeable differences in precipitation on days with and without ARs (not shown); however, the average precipitation at the two northerly stations was noticeably higher on EDP days that occur on SBJ days ( $N = 45$ ; 57 mm) as compared to non-SBJ days ( $N = 5$ ; 29 mm). These results are constrained by a total sample size of 50 days and subsample sizes that are fewer than 5–10 days, and the data are not very suitable for a rigorous statistical analysis. These results do, however, suggest that EDP across the more northern region of the upper Sacramento River watershed in proximity to the Mt. Shasta–Trinity Alps region may be noticeably influenced by the presence of an SBJ, which could be tested for statistical significance with a larger dataset. The EDP in this region in association with the SBJ could therefore have a significant impact on water resource management, for example, at California's largest reservoir at Shasta Lake behind Shasta Dam (Fig. 1).

The findings presented in this paper suggest that accurate forecasts of EDP in the upper Sacramento River watershed are influenced in part by how well prediction systems resolve both synoptic- and mesoscale processes over Northern California in conjunction with landfalling ARs and the SBJ. For example, the terrain-induced positive elevation bias in the altitude of maximum wind speed along the SBJ and negative magnitude bias in water vapor flux along the SBJ identified by Hughes et al. (2012) in NARR as compared to higher-resolution downscaled simulations indicates that a weather prediction model capable of accurately resolving the terrain across California and attendant synoptic- and terrain-induced mesoscale circulations will likely perform better at forecasting EDP than a lower-resolution model. Given the complex nature of the terrain and terrain-induced mesoscale circulations, it is recommended that future forecast system enhancements include both detailed monitoring and prediction of landfalling ARs and the SBJ in this region. Given the established linkages

between ARs and SBJs (e.g., Kingsmill et al. 2013; Neiman et al. 2013, 2014), between ARs and streamflow (e.g., Neiman et al. 2011), and between SBJs and streamflow (e.g., Neiman et al. 2014), this effort would enable short lead time refinements to reservoir operations under potential flood conditions, as documented during the Howard Hanson Dam flood-risk crisis in Washington (White et al. 2012), and could be achieved as an expansion of the Enhanced Flood Response and Emergency Preparedness observing network recently installed in California (White et al. 2013; Ralph et al. 2014).

*Acknowledgments.* This research was supported by funding provided by Award 4600010378 through the California Department of Water Resources. Comments by three anonymous reviewers greatly improved the quality of this manuscript.

#### REFERENCES

- Carter, D. A., K. S. Gage, W. L. Ecklund, W. M. Angevine, P. E. Johnston, A. C. Riddle, J. S. Wilson, and C. R. Williams, 1995: Developments in UHF lower tropospheric wind profiling at NOAA's Aeronomy Laboratory. *Radio Sci.*, **30**, 977–1001, doi:10.1029/95RS00649.
- Dettinger, M. D., 2004: Fifty-two years of "Pineapple-Express" storms across the west coast of North America. PIER Project Rep. CEC-500-2005-004, California Energy Commission, 20 pp. [Available online at <http://www.energy.ca.gov/2005publications/CEC-500-2005-004/CEC-500-2005-004.PDF>.]
- , F. M. Ralph, T. Das, P. J. Neiman, and D. Cayan, 2011: Atmospheric rivers, floods, and the water resources of California. *Water*, **3**, 445–478, doi:10.3390/w3020445.
- Galewsky, J., and A. Sobel, 2005: Moist dynamics and orographic precipitation in northern and central California during the New Year's Flood of 1997. *Mon. Wea. Rev.*, **133**, 1594–1612, doi:10.1175/MWR2943.1.
- Guan, B., N. Molotch, D. Waliser, E. Fetzer, and P. J. Neiman, 2010: Extreme snowfall events linked to atmospheric rivers and surface air temperature via satellite measurements. *Geophys. Res. Lett.*, **37**, L20401, doi:10.1029/2010GL044696.
- Hollinger, J. P., J. L. Peirce, and G. A. Poe, 1990: SSM/I instrument evaluation. *IEEE Trans. Geosci. Remote Sens.*, **28**, 781–790, doi:10.1109/36.58964.
- Hughes, M., P. J. Neiman, E. Sukovich, and F. M. Ralph, 2012: Representation of the Sierra barrier jet in 11 years of a high-resolution dynamical reanalysis downscaling. *J. Geophys. Res.*, **117**, D18116, doi:10.1029/2012JD017869.
- Kim, J., and H.-S. Kang, 2007: The impact of the Sierra Nevada on low-level winds and water vapor transport. *J. Hydrometeorol.*, **8**, 790–804, doi:10.1175/JHM599.1.
- , D. E. Waliser, P. J. Neiman, B. Guan, J.-M. Ryoo, and G. A. Wick, 2012: Effects of atmospheric river landfalls on the cold season precipitation in California. *Climate Dyn.*, **38**, 411–429, doi:10.1007/s00382-010-0972-2.
- Kingsmill, D. E., P. J. Neiman, B. J. Moore, M. Hughes, S. E. Yuter, and F. M. Ralph, 2013: Kinematic and thermodynamic structures of Sierra barrier jets and overrunning atmospheric rivers during a land-falling winter storm in Northern California. *Mon. Wea. Rev.*, **141**, 2015–2036, doi:10.1175/MWR-D-12-00277.1.
- Lundquist, J. D., J. R. Minder, P. J. Neiman, and E. M. Sukovich, 2010: Relationships between barrier jet heights, precipitation distributions, and streamflow in the northern Sierra Nevada. *J. Hydrometeorol.*, **11**, 1141–1156, doi:10.1175/2010JHM1264.1.
- Mesinger, F., and Coauthors, 2006: North American Regional Reanalysis. *Bull. Amer. Meteor. Soc.*, **87**, 343–360, doi:10.1175/BAMS-87-3-343.
- Minder, J. R., D. R. Durran, and G. H. Roe, 2011: Mesoscale controls on the mountainside snow line. *J. Atmos. Sci.*, **68**, 2107–2127, doi:10.1175/JAS-D-10-05006.1.
- Neiman, P. J., F. M. Ralph, G. A. Wick, Y.-H. Kuo, T.-K. Wee, Z. Ma, G. H. Taylor, and M. D. Dettinger, 2008a: Diagnosis of an intense atmospheric river impacting the Pacific Northwest: Storm summary and offshore vertical structure observed with COSMIC satellite retrievals. *Mon. Wea. Rev.*, **136**, 4398–4420, doi:10.1175/2008MWR2550.1.
- , —, —, J. Lundquist, and M. D. Dettinger, 2008b: Meteorological characteristics and overland precipitation impacts of atmospheric rivers affecting the West Coast of North America based on eight years of SSM/I satellite observations. *J. Hydrometeorol.*, **9**, 22–47, doi:10.1175/2007JHM855.1.
- , E. M. Sukovich, F. M. Ralph, and M. Hughes, 2010: A seven-year wind profiler-based climatology of the windward barrier jet along California's northern Sierra Nevada. *Mon. Wea. Rev.*, **138**, 1206–1233, doi:10.1175/2009MWR3170.1.
- , L. J. Schick, F. M. Ralph, M. Hughes, and G. A. Wick, 2011: Flooding in western Washington: The connection to atmospheric rivers. *J. Hydrometeorol.*, **12**, 1337–1358, doi:10.1175/2011JHM1358.1.
- , M. Hughes, B. J. Moore, F. M. Ralph, and E. S. Sukovich, 2013: Sierra barrier jets, atmospheric rivers, and precipitation characteristics in Northern California: A composite perspective based on a network of wind profilers. *Mon. Wea. Rev.*, **141**, 4211–4233, doi:10.1175/MWR-D-13-00112.1.
- , F. M. Ralph, B. J. Moore, and B. J. Zamora, 2014: The regional influence of an intense Sierra barrier jet and landfalling atmospheric river on orographic precipitation in Northern California: A case study. *J. Hydrometeorol.*, **15**, 1419–1439, doi:10.1175/JHM-D-13-0183.1.
- Parish, T. R., 1982: Barrier winds along the Sierra Nevada Mountains. *J. Appl. Meteor.*, **21**, 925–930, doi:10.1175/1520-0450(1982)021<0925:BWATSN>2.0.CO;2.
- Ralph, F. M., and M. D. Dettinger, 2012: Historical and national perspectives on extreme West Coast precipitation associated with atmospheric rivers during December 2010. *Bull. Amer. Meteor. Soc.*, **93**, 783–790, doi:10.1175/BAMS-D-11-00188.1.
- , P. J. Neiman, and G. A. Wick, 2004: Satellite and CALJET aircraft observations of atmospheric rivers over the eastern North Pacific Ocean during the winter of 1997/98. *Mon. Wea. Rev.*, **132**, 1721–1745, doi:10.1175/1520-0493(2004)132<1721:SACAOO>2.0.CO;2.
- , —, —, S. I. Gutman, M. D. Dettinger, D. R. Cayan, and A. B. White, 2006: Flooding on California's Russian River: The role of atmospheric rivers. *Geophys. Res. Lett.*, **33**, L13801, doi:10.1029/2006GL026689.
- , —, G. N. Kiladis, K. Weickmann, and D. M. Reynolds, 2011: A multi-scale observational case study of a Pacific atmospheric river exhibiting tropical–extratropical connections and a mesoscale frontal wave. *Mon. Wea. Rev.*, **139**, 1169–1189, doi:10.1175/2010MWR3596.1.

- , —, R. J. Zamora, and M. D. Dettinger, 2013a: Observed impacts of duration and seasonality of atmospheric-river landfalls on soil moisture and runoff in coastal Northern California. *J. Hydrometeor.*, **14**, 443–459, doi:[10.1175/JHM-D-12-076.1](https://doi.org/10.1175/JHM-D-12-076.1).
- , and Coauthors, 2013b: The emergence of weather-focused testbeds linking research and forecasting operations. *Bull. Amer. Meteor. Soc.*, **94**, 1187–1210, doi:[10.1175/BAMS-D-12-00080.1](https://doi.org/10.1175/BAMS-D-12-00080.1).
- , and Coauthors, 2014: A vision for future observations for western U.S. extreme precipitation and flooding. *J. Contemp. Water Res. Educ.*, **153**, 16–32, doi:[10.1111/j.1936-704X.2014.03176.x](https://doi.org/10.1111/j.1936-704X.2014.03176.x).
- Reeves, H. D., Y.-L. Lin, and R. Rotunno, 2008: Dynamic forcing and mesoscale variability of heavy precipitation events over the Sierra Nevada Mountains. *Mon. Wea. Rev.*, **136**, 62–77, doi:[10.1175/2007MWR2164.1](https://doi.org/10.1175/2007MWR2164.1).
- Smith, B. L., S. E. Yuter, P. J. Neiman, and D. E. Kingsmill, 2010: Water vapor fluxes and orographic precipitation over Northern California associated with a land-falling atmospheric river. *Mon. Wea. Rev.*, **138**, 74–100, doi:[10.1175/2009MWR2939.1](https://doi.org/10.1175/2009MWR2939.1).
- Wentz, F. J., 1995: The intercomparison of 53 SSM/I water vapor algorithms. Remote Sensing Systems Tech. Rep., 19 pp.
- White, A. B., and Coauthors, 2012: NOAA's Rapid Response to the Howard A. Hanson Dam flood risk management crisis. *Bull. Amer. Meteor. Soc.*, **93**, 189–207, doi:[10.1175/BAMS-D-11-00103.1](https://doi.org/10.1175/BAMS-D-11-00103.1).
- , and Coauthors, 2013: A twenty-first-century California observing network for monitoring extreme weather events. *J. Atmos. Oceanic Technol.*, **30**, 1585–1603, doi:[10.1175/JTECH-D-12-00217.1](https://doi.org/10.1175/JTECH-D-12-00217.1).
- , P. J. Neiman, J. M. Creamean, T. Coleman, F. M. Ralph, and K. A. Prather, 2015: The impacts of California's San Francisco Bay Area gap on precipitation observed in the Sierra Nevada during HMT and CalWater. *J. Hydrometeor.*, **16**, 1048–1069, doi:[10.1175/JHM-D-14-0160.1](https://doi.org/10.1175/JHM-D-14-0160.1).
- Zhu, Y., and R. E. Newell, 1998: A proposed algorithm for moisture fluxes from atmospheric rivers. *Mon. Wea. Rev.*, **126**, 725–735, doi:[10.1175/1520-0493\(1998\)126<0725:APAFMF>2.0.CO;2](https://doi.org/10.1175/1520-0493(1998)126<0725:APAFMF>2.0.CO;2).